Constraints on the dipole photon strength functions from experimental multistep cascade spectra

M. Krtička,[1] S. Goriely,[2] S. Hilaire,[3] S. Péru,[3] and S. Valenta[1]
[1]*Faculty of Mathematics and Physics, Charles University, 180 00 Prague, Czech Republic*
[2]*Institut d'Astronomie et d'Astrophysique, Université Libre de Bruxelles, CP-226, 1050 Brussels, Belgium*
[3]*CEA, DAM, DIF, F-91297 Arpajon, France*

(Received 11 December 2018; revised manuscript received 11 January 2019; published 15 April 2019)

Viable theoretical predictions of photon strength functions (PSFs) covering the whole nuclear chart are of great interest for different nuclear applications, including, in particular, nuclear astrophysics. Recently, such a global PSF model consisting of axially deformed Hartree-Fock-Bogolyubov (HFB) + quasiparticle random phase approximation (QRPA) calculations with the D1M Gogny interaction and a phenomenological low-energy contribution was proposed. In the present paper, we test this model predictions against previously published data from measurements of multistep γ cascades following neutron capture on isolated resonances performed with the DANCE detector. Such data present a stringent test of the PSFs models, in particular for the properties of the $M1$ scissors mode and the possible low-energy PSFs enhancement. A detailed comparison is made for spectra obtained from resonances for spherical, quasispherical, and well-deformed nuclei. This comparison indicates that the location and strength of the scissors mode is reasonably described by the HFB + QRPA approach. Moreover, a low-energy PSF contribution, not predicted by the HFB + QRPA calculation of the photoabsorption PSF, should be present in all nuclei. A systematics of this low-energy contribution, assumed in the $M1$ PSF, is proposed.

DOI: 10.1103/PhysRevC.99.044308

I. INTRODUCTION

Radiative neutron capture cross sections play a key role in many nuclear applications. Despite a huge experimental effort, theoretical predictions are required to fill the gaps, in particular for nuclei for which measurements are not feasible at the present time. This is especially the case of nuclear astrophysics, which requires the determination of radiative neutron capture cross sections for a large number of exotic neutron-rich nuclei [1]. To describe nuclei far away from the experimentally known region, large-scale calculations need to be performed on the basis of models that are definitely able to describe available data.

The neutron capture cross sections are commonly evaluated within the framework of the Hauser-Feshbach statistical model, although the direct capture contribution plays an important role for very exotic nuclei [2]. The (n, γ) cross section strongly depends on the photon de-excitation probability, which is within the statistical model described via photon strength functions (PSFs) for different transition types (electric E or magnetic M) and multipolarities L, the dipole transitions ($L = 1$) being the dominant ones. Both $E1$ and $M1$ types have been traditionally modelled by the phenomenological Lorentzian approximation or, for $E1$, sometimes via its excitation-energy-dependent variants, such as the widely used generalized Lorentzian (GLO) model [3–5].

The reliability of the PSF predictions can be greatly improved by the use of microscopic or semimicroscopic models. Such an effort has recently been made and a complete set of $E1$ and $M1$ PSFs was derived from the mean field plus quasiparticle random phase approximation (QRPA) calculations in Refs. [6–11]. When compared to experimental data and considered for practical applications, these QRPA calculations need, however, some phenomenological corrections. These include a broadening of the QRPA strength to take into account the neglected damping of collective motions as well as a shift of the strength to lower energies due to the contribution beyond the 1 particle-1 hole (1p1h) excitations and the interaction between the single-particle and low-lying collective phonon degrees of freedom [12–19]. In addition, most of the QRPA calculations assume spherical symmetries, so that phenomenological corrections need to be included to properly describe the splitting of the giant electric-dipole resonance (GEDR) in deformed nuclei [6]. State-of-the-art calculations including effects beyond the 1p1h excitations and phonon coupling are now available [12–19] but they remain computer-wise intractable for large-scale applications.

Recently, axially deformed Hartree-Fock-Bogolyubov (HFB) plus QRPA calculations based on the finite-range D1M Gogny interaction, hereafter referred to as D1M + QRPA, have been shown to provide rather satisfactory predictions of the properties of the GEDR [9] as well as of the $M1$ PSF at energies lower or comparable to the neutron separation energy S_n [10]. Such QRPA calculations give only transitions from the ground to the excited states, so their application to the description of the γ decay between excited states requires additional assumptions. Usually, it is assumed that the electromagnetic response of a nucleus depends only on the γ-ray energy ε_γ; this assumption is known as the Brink hypothesis [20]. In reality, a nonzero limit of the dipole strength for transitions between excited states has been

reported from experiment [21,22] and later proposed also from the shell model (SM) calculations [23–29]. For this reason, the D1M + QRPA calculations were complemented with a phenomenological low-ε_γ contribution both for the $E1$ and $M1$ strengths; this extended model is referred to as D1M + QRPA + 0lim. Such a low-energy contribution of the dipole PSFs, inspired partly by the SM calculations, remains, however, not fully understood in many aspects. For instance, systematic SM calculations for light $A \lesssim 80$ nuclei [26–29] suggest that the overall strength of the low-ε_γ $M1$ contribution and its energy dependence may vary with deformation, but little experimental constraints exist. Also a clear experimental evidence for the $E1$ or $M1$ character of the strength at $\varepsilon_\gamma \to 0$ is missing. Available experimental data seem to indicate that contribution of both transition types can be expected [22,30].

Most of the theoretical models have been tuned on experimental data that are believed to give "direct" information on the PSFs. These include photoabsorption experiments [31–34], nuclear resonance fluorescence (NRF) [35,36], reaction data analysis with the Oslo method [37–39], as well as average (ARC) and discrete (DRC) neutron resonance capture data [40]. Very often also the average radiative widths [5] are used to check the PSF models although there is a significant influence of the level density (LD) on this quantity.

In reality, data on two-step [41–43] and multistep γ cascade (MSC) spectra [44–51] from radiative neutron capture can also be used for constraining or tuning the PSFs models. In these cases, the PSFs cannot be directly extracted from experimental data but tested and validated through a comparison between experimental data and their simulated counterparts based on different PSFs and LD models. In this paper we perform a systematic comparison between results predicted by the D1M + QRPA + 0lim model [11] and the MSC spectra for all nuclei that have been published up to now from measurements with the DANCE detector. It should be stressed that our aim is not to tune the model parameters for each nucleus but to test its global validity and possibly get a simple systematics for unknown parameters present in the model that are loosely constrained at the moment.

The D1M + QRPA + 0lim PSF model is described in Sec. II emphasizing some of its aspects that have not been strictly constrained in the past. Section III gives a short description of experimental spectra and production of their analogues from simulations with this PSF model. In Sec. IV experimental multiplicity distribution (MD) and MSC spectra are compared to predictions from simulations with different ingredients affecting either the PSFs or the LD model. These comparisons are performed for the 15 nuclei for which data are available. A discussion of results and comparison of data to predictions based on the traditionally used phenomenological PSF model are presented in Sec. V. Impacts of the D1M + QRPA + 0lim results on the Maxwellian-averaged cross section are given in Sec. VI and conclusions are finally drawn in Sec. VII.

II. THEORETICAL PHOTON STRENGTH FUNCTIONS

All details about the D1M + QRPA + 0lim model can be found in Refs. [9,11,52,53] and only a brief summary is given here. The $E1$ and $M1$ PSFs for de-excitation $\overleftarrow{f}(\varepsilon_\gamma)$, including the phenomenological low-energy contributions, are expressed as

$$\overleftarrow{f}_{E1}(\varepsilon_\gamma) = f_{E1}^{\mathrm{QRPA}}(\varepsilon_\gamma) + \frac{f_0 U}{1 + e^{(\varepsilon_\gamma - \varepsilon_0)}}, \tag{1}$$

$$\overleftarrow{f}_{M1}(\varepsilon_\gamma) = f_{M1}^{\mathrm{QRPA}}(\varepsilon_\gamma) + C\, e^{-\eta \varepsilon_\gamma}, \tag{2}$$

where f_{X1}^{QRPA} is the D1M + QRPA dipole strength ($X = E$ or M) at the photon energy ε_γ, U (in MeV) is the excitation energy of the initial state, and f_0, ε_0, C and η are free parameters of the phenomenological low-ε_γ limit contribution that were adjusted up to now using the SM results and available low-ε_γ experimental data such as those obtained with the Oslo method [21,37,54] or the average radiative widths [5]. Values of $f_0 \simeq 1 - 5 \times 10^{-10}$ MeV^{-4}, $\varepsilon_0 \simeq 3 - 5$ MeV, $C \simeq 1 - 3 \times 10^{-8}$ MeV^{-3}, and $\eta = 0.8$ MeV^{-1} were adopted in Ref. [11].

As far as the D1M + QRPA calculation of the dipole strength is concerned, the effects beyond the 1p1h QRPA have been empirically taken into account by folding the QRPA strength with a Lorentzian-type function, considering an energy shift that increases with energy and a broadening of the strength that may vary with the isotope mass and/or quadrupole deformation.

The renormalization procedure to reproduce both the experimental GEDR centroid energy and low-energy vibrational states includes an energy shift of $\Delta = 0.5$ MeV for $\varepsilon_\gamma \leqslant 0.5$ MeV, $\Delta = 2.5$ MeV for $\varepsilon_\gamma = 18$ MeV and $\Delta = 5$ MeV for $\varepsilon_\gamma \geqslant 21$ MeV. For energies in the $0.5 \leqslant \varepsilon_\gamma \leqslant 21$ MeV range, the energy shift Δ is interpolated linearly between the anchor values at 0.5, 18, and 21 MeV. Both the $E1$ and $M1$ D1M + QRPA strengths are shifted by the same energy Δ.

An empirical damping of the collective motions is introduced by folding the D1M + QRPA strength with a Lorentzian function with the broadening width Γ_{X1}. For the $E1$ PSF, Γ has been adjusted on photoabsorption data and assumed to differ for both possible projections K of the angular momentum. More precisely, in even-even nuclei the width is expressed as $\Gamma_{E1}(K = 0^-) = \Gamma_0/(1 + \beta_{20})$ and $\Gamma_{E1}(K = 1^-) = \Gamma_0 \times (1 + \beta_{20})$, where Γ_0 [MeV] $= 7 - A/45$ for $A \leqslant 200$, and 2.5 MeV otherwise and β_{20} is the axial quadrupole deformation parameter. For the $M1$ strength, a constant value of $\Gamma_{M1} = 0.5$ MeV was arbitrarily adopted [10] because of the lack of experimental data able to constrain the width of the $M1$ resonance structures in contrast to the $E1$ component for which hundreds of photonuclear data [34] are available to provide the above-described systematics [9]. Note that none of the D1M + QRPA PSFs calculations were performed for odd-A and odd-odd nuclei. To estimate PSFs in these nuclei the same interpolation procedure as the one described in Ref. [9] was applied.

The D1M + QRPA + 0lim model was checked against a wide range of experimental data, from the lowest energies to the GEDR region, that include photonuclear data as well as ARC, DRC, NRF, Oslo-type data or integrated quantities such as average radiative width or radiative neutron capture cross sections [11]. Despite the relatively good description of

this data, some model parameters remain loosely constrained. This concerns, in particular, the broadening width of the $M1$ component, arbitrarily proposed to be $\Gamma_{M1} = 0.5$ MeV and the amplitude of the low-ε_γ $M1$ enhancement adjusted to $C \simeq 1 - 3 \times 10^{-8}$ MeV^{-3} in Ref. [11] following the analysis of Oslo data at energies below about 2 MeV [39] as well as the SM predictions for light nuclei [25,29].

As shown below, the MSC data from isolated resonances can provide stringent tests of the overall quality of the $E1$ and $M1$ PSFs from this model for $\varepsilon_\gamma < S_n$ and further constraints the C and Γ_{M1} parameters. The low-ε_γ $E1$ contribution is also poorly constrained but at $\varepsilon_\gamma \lesssim 2 - 3$ MeV the decay is expected to be dominated by the $M1$ PSF component, so that the $E1$ contribution plays a minor role.

III. EXPERIMENTAL DATA AND SIMULATIONS

A. Experiment

Predictions based on the above-introduced PSF model are in this paper compared to γ-ray data from the decay of strong, well-resolved resonances with known spin and parity measured by the DANCE detector [55,56]. The DANCE detector is a highly segmented highly efficient (≈85% for a 1 MeV γ ray) array consisting of 160 BaF_2 crystals that cover a solid angle of $\approx 3.5\pi$.

Neutrons with different energies, produced by pulsed proton beam impinging onto the spallation target at the Manuel Lujan Jr. Neutron Scattering Center (LANSCE) [57] at the Los Alamos National Laboratory, interact with usually isotopically enriched sample placed in the center of the detector. Each crystal of the detector array serves as a spectrometer for detection of γ rays emitted in the decay of individual neutron resonance that can be identified using the time-of-flight technique as the detector is located at 20 m from the spallation target.

B. Data reduction

Details of extraction of various types of spectra from experimental data were described elsewhere [44–51]. Here we list only basic facts related to the spectra compared in this paper.

High segmentation of the DANCE detector array allows to sort γ cascades following the radiative neutron capture according to the detected multiplicity. In reality, individual γ-rays do not necessarily deposit their full energy in a single crystal, but often several neighboring crystals [58]. To bring the detected multiplicity closer to the real one and make some structures in the MSC spectra more pronounced, we combined all firing contiguous crystals into a cluster. The number of clusters in a capture event is called the cluster multiplicity M and individual detected events are sorted according to this quantity. Although we use only the cluster multiplicity, the conclusions presented below do not change whether the crystal (number of firing crystals) or the cluster multiplicity is used.

Two observables from the γ decay of individual resonances are used for comparison in this paper. Both were constructed with a help of so-called sum-energy spectra constructed from

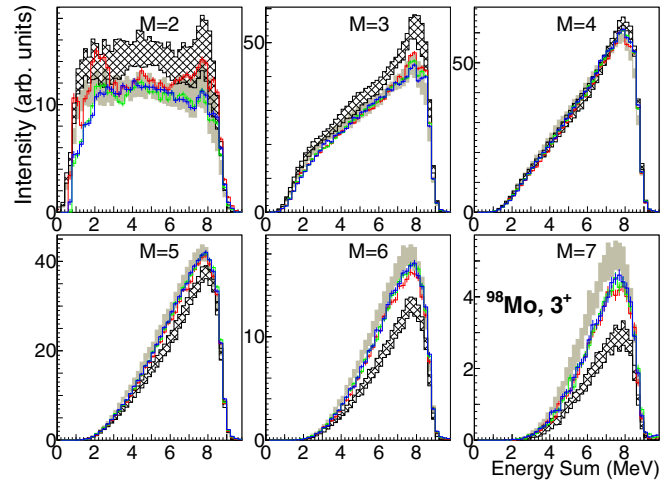

FIG. 1. Sum-energy spectra from decay of 3^+ resonances in ^{98}Mo. The color histograms correspond to experimental data from three different resonances, the black hatched area and the gray band to predictions (average ± standard deviation) from simulations with $C = 1 \times 10^{-8}$ MeV^{-3} and $C = 3 \times 10^{-8}$ MeV^{-3}, respectively. See text for details.

the sum of deposited energies of γ-rays from a given cascade. These spectra for different multiplicities M, from decay of 3^+ resonances produced in the ^{97}Mo(n, γ)^{98}Mo reaction, are shown in Fig. 1. The MD and MSC spectra [44,50] from cascades with deposited sum energy in the E_Σ range near the neutron separation energy S_n, were then constructed. The exact used E_Σ range is for each nucleus listed in Table I.

As indicated by Fig. 1, the spectral shape of the sum-energy spectra from simulations is often very similar to the experimental shape for a range of PSFs and LD models. The main information on the γ decay in these spectra is thus observed MD. We therefore decided to replace the sum-energy spectra with more compact MD spectra. Although Fig. 1 indicates that we might use rather wide E_Σ range, restriction only to events in the relatively narrow E_Σ range near S_n allows us to suppress a possible contribution of the background and impurities in the target. The MD plot corresponding to the spectra in Fig. 1 can be found in Fig. 2(d).

For a given resonance, an experimental MSC spectrum for multiplicity M was constructed by incrementing counts in M bins corresponding to the γ-ray energies deposited in the M individual clusters within an event. Adopted E_Σ ranges in this work are identical to ranges used in original works on MSC spectra listed in Table I. The spectra from different neutron resonances are normalized to the same total number of detected events in the E_Σ range for $M = 2 - 7$ ($M = 2 - 6$ in U isotopes) in the sum-energy spectra.

Energies of individual shown resonances for each product nucleus and resonance spin are listed in the Supplemental Material [59]; two to four resonances with the same spin in a given nucleus are compared. In some nuclei we have spectra with sufficient statistics from more resonances. In these cases, the chosen set of shown resonances should represent well the whole available sample. The MDs from individual resonances are shown below as color symbols. The corresponding

TABLE I. Different characteristics of isotopes used in comparison. Original papers with the analysis of MSC spectra are listed in the first column. The quadrupole deformation parameter β_{20} corresponds to the D1M prediction [60]. The last column gives estimates of allowed values of the parameter C, describing the zero-ε_γ limit of the $M1$ PSF in the D1M + QRPA + 0lim model. Cases labeled by * show significant differences in spectral shapes between experiment and simulations. For more details on allowed C values and E_Σ range, see text.

Isotope	β_{20}	J^π	E_Σ [MeV]	$C[10^{-8}$ MeV$^{-3}]$
^{96}Mo [44]	0.00	2^+	7.6–9.2	2.3–3.5
		3^+		2.0–3.4
		2^-		1.5–5.0
		3^-		1.5–5.0
^{98}Mo [45]	0.18	2^+	8.2–9.2	2.0–3.5
		3^+		2.0–3.0
^{112}Cd [46]	0.14	0^+	9.2–9.6	0.5–1.8*
		1^+		0.4–1.0
^{114}Cd [46]	0.15	0^+	8.8–9.2	0.7–1.6
		1^+		0.3–1.0
^{153}Gd [47]	0.24	$1/2^+$	5.4–6.4	0.6–1.3
^{155}Gd [47]	0.34	$1/2^+$	5.8–6.6	0.3–0.8
^{157}Gd [47]	0.33	$1/2^+$	5.4–6.5	0.3–1.3
^{159}Gd [47]	0.34	$1/2^+$	5.2–6.2	0.3–1.5
^{156}Gd [48]	0.33	1^-	7.2–8.6	1.2–2.2
		2^-		0.8–1.5
^{158}Gd [49]	0.34	1^-	7.0–8.1	1.2–2.5
		2^-		1.0–2.0
^{162}Dy [50]	0.34	2^+	7.6–8.4	1.0—2.0*
		3^+		0.7–1.7*
^{164}Dy [50]	0.34	2^-	7.0–7.8	0.1–1.1
		3^-		<1.0*
^{235}U [51]	0.27	$1/2^+$	4.8–5.8	0.6–1.2
^{237}U [51]	0.27	$1/2^+$	4.63–5.63	0.6–1.5
^{239}U [51]	0.28	$1/2^+$	4.16–5.16	0.7–1.2

experimental MSC spectra are then plotted as histograms of the respective colors. Differences in spectra from individual neutron resonances arise from fluctuations of primary transitions (which are expected to follow the Porter-Thomas distribution [61]). In reality, as evident from presented figures the difference in the MD from different resonances of the same spin and parity is usually small.

C. Simulations of spectra

The MD and MSC spectra measured with the DANCE detector are products of a complex interplay between the PSFs of different types, LD and detector response to individual cascades. As a result, the PSFs cannot be directly extracted from the experimental spectra. However, predictions based on different models (or model parameters) of PSFs and LD can be compared to experimental data.

Indeed, utilizing the Monte Carlo DICEBOX algorithm [62], the γ cascades following the resonant neutron capture can be generated under various assumptions about the PSFs and LD. The DICEBOX code allows to treat correctly the expected

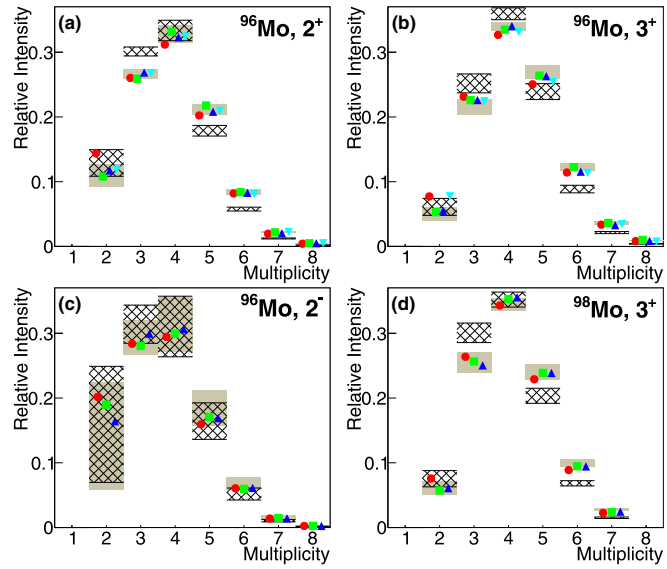

FIG. 2. The MD from the decay of ^{96}Mo and ^{98}Mo resonances. The color symbols correspond to experimental data from different resonances, the black hatched area and the gray band to predictions from simulations (average ± one standard deviation) with $C = 1 \times 10^{-8}$ MeV^{-3} and $C = 3 \times 10^{-8}$ MeV^{-3}, respectively. See text for details.

Porter-Thomas fluctuations of partial radiation widths via the concept of *nuclear realizations* – different sets of all levels and partial radiation widths in a simulated nucleus. Individual nuclear realizations yield different predictions of observables even for a fixed combination of the PSFs and LD models and the spin and parity of the capturing state. For each tested combination of the PSFs and LD models, we simulated 15 different nuclear realizations.

The response of the DANCE detector to each simulated cascade was then determined using the Monte-Carlo GEANT4-based code [58]. The sum-energy spectra, MD, and MSC spectra were constructed separately for each nuclear realization analogously to experimental data. Predictions from individual nuclear realizations were again normalized to give the same area in the E_Σ range of the sum-energy spectra for $M = 2$–7 (2–6 in U isotopes). The range of predictions corresponding to two standard deviations (average ± standard deviation) from individual nuclear realizations with a fixed combination of the PSFs and LD models is shown in the figures. For comparison purposes, the results from two different simulations are plotted in each figure, one as a black hatched and the other as a gray band.

The absolute normalization of experimental and simulated MD spectra is via the sum of contributions for $M = 2$–7, which is equal to unity. Simulated MSC spectra are normalized to experimental ones using one (common for all M) normalization factor, again to give the same area in the sum-energy spectra for $M = 2$–7. The absolute scale on the vertical axes of presented figures with MSC spectra is arbitrary but the relative contributions of different Ms are kept.

The bin width was chosen separately for each isotope. As a first condition, we require sufficiently high statistics

in experimental spectra. If this condition is fulfilled even for very small bin widths, we choose the bins wide enough to either keep the fluctuations in predictions from different nuclear realizations relative small or to be close to the energy resolution of the crystals. It turns out that the appropriate bin widths for the MSC spectra in this paper are between 100 and 250 keV.

IV. COMPARISON BETWEEN EXPERIMENT AND PREDICTIONS

In this section, experimental MD and MSC spectra are compared to predictions from simulations with different ingredients affecting either the D1M + QRPA + 0lim PSFs or LD model. Specifically, we varied in simulations the size of the $M1$ zero-ε_γ amplitude C (Sec. IV A), the $M1$ broadening width Γ_{M1} (Sec. IV B) and the $E1$ low-ε_γ limit given by the f_0 and ε_0 parameters (Sec. IV C). If not explicitly mentioned, simulations are performed with $f_0 = 1 \times 10^{-10}$ MeV^{-4}, $\varepsilon_0 = 3$ MeV, and $\Gamma_{M1} = 0.5$ MeV.

Both the MD and MSC spectra can be also sensitive to the adopted LD model. To check this sensitivity two rather different LD prescriptions are considered, namely the microscopically based HFB plus combinatorial model [63] and the phenomenological constant temperature (CT) plus Fermi gas model [64] recommended by the Reference Input Parameter Library RIPL-3 [5]. Below we usually refer to these two models as to the "combinatorial" and "CT," respectively. Both these LD models are normalized using existing s-wave spacing data at S_n and the cumulative number of known low-lying levels [5]. The vast majority of our simulations are performed with the combinatorial model, for simulations with the CT model see Sec. IV D.

A. Sensitivity to $M1$ low-ε_γ amplitude C

Figures 2 to 8 compare experimental and simulated MD and MSC spectra for selected nuclei and resonance spins for two values of C – the gray band corresponds to $C = 3 \times 10^{-8}$ MeV^{-3}, while the hatched area between the black lines to $C = 1 \times 10^{-8}$ MeV^{-3}; figures for all tested nuclei and resonance spins can be found in the Supplemental Material [59]. Different predictions with these two values of C imply that experimental spectra are sensitive to this parameter.

Not surprisingly, the MD with $C = 1 \times 10^{-8}$ MeV^{-3} is shifted toward lower values with respect to that with $C = 3 \times 10^{-8}$ MeV^{-3}. It should be stressed that a reproduction of the experimental MD is a necessary but not a sufficient condition for an acceptable description of the decay. The experimental and simulated MSC spectra for individual M's can have a different shape even if their MD is similar. Figures 3 to 8 indicate that the predicted shape of MSC spectra for individual Ms is in most cases similar for both values of C, they differ in the magnitude. The MSC spectra for $M > 5$ are then usually structureless for $\varepsilon_\gamma \gtrsim 1$ MeV.

Globally, it is found that simulations with the D1M + QRPA + 0lim PSF can describe experimental spectra rather satisfactorily, provided the amplitude C of the $M1$ zero-ε_γ limit is adjusted within a certain range. The upper and lower limits on C, listed in Table I, lead to acceptable description of the experimental spectra and were determined from simulations with a rather detailed grid of the parameter. Deduced C values – that should be considered as (probably rather

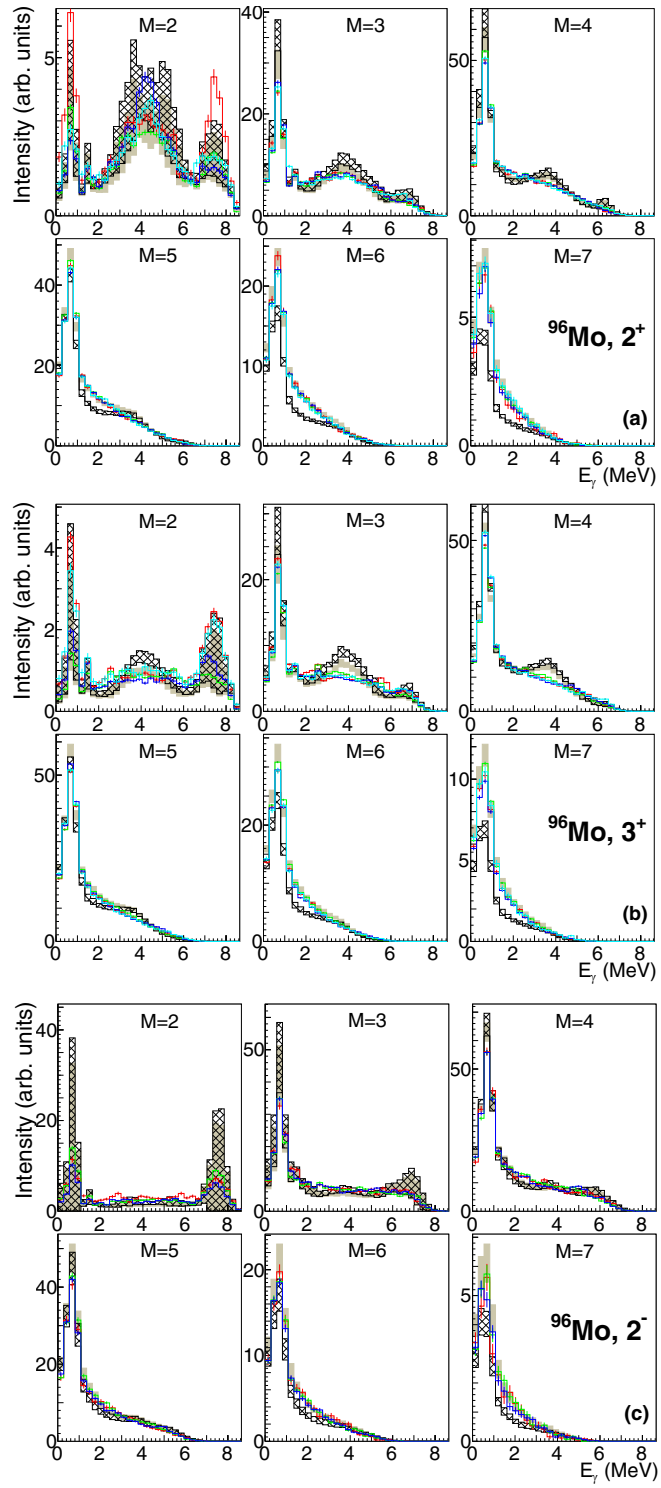

FIG. 3. The MSC spectra from ^{96}Mo resonances with different spins and parities. The color symbols correspond to experimental data, the black hatched area and the gray band to predictions from simulations (average ± one standard deviation) with $C = 1 \times 10^{-8}$ MeV^{-3} and $C = 3 \times 10^{-8}$ MeV^{-3}, respectively.

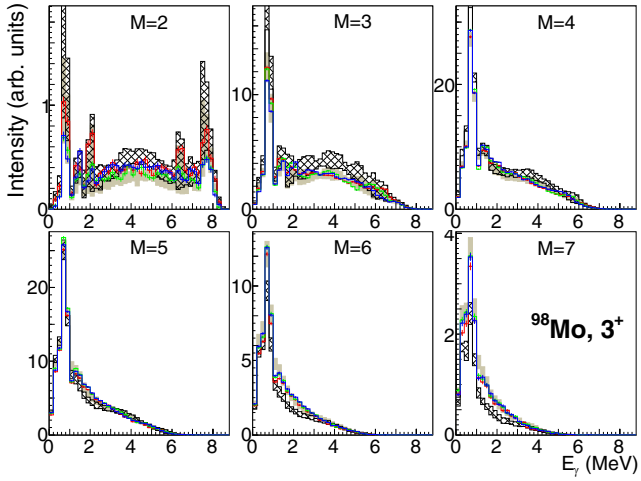

FIG. 4. The same as in Fig. 3 but for the MSC spectra from 3^+ resonances in ^{98}Mo.

conservative) upper and lower limits – are based mainly on a visual comparison. We have not applied any traditional statistical criterion for correct constraining values of C as (i) there is an unknown nontrivial correlation among spectra for different multiplicities [44,50] and (ii) the checked model is clearly not perfect, as can be expected from any global model without a fine tuning, see Figs. 3 to 8. However, values of the "effective" χ^2 criterion (neglecting any correlation) give minimum values for C values close the center of the interval listed in Table I. In any case, the prediction of the D1M + QRPA + 0lim model is in majority of tested isotopes significantly better than with other widely used PSFs models, see Sec. V B, and its imperfections do not strongly impact our sensitivity to the size of the phenomenological low-ε_γ enhancement.

In a few nuclei the imperfections of the prediction of MSC spectra are rather significant. The most pronounced cases are labeled with the symbol * in Table I. The listed range of C values in these cases are based only on MD for $M > 2$ as the most pronounced disagreement between experiment and simulations is often visible in the $M = 2$ MSC spectra. Probably the most pronounced disagreement is seen in the $M = 2$–4 MSC spectra from the decay of 0^+ resonances of ^{112}Cd (Fig. 5), and in the decay of ^{162}Dy (Fig. 7 and Supplemental Material [59]). These differences might come from other quantities involved in γ decay, such as LD, different low-ε_γ limit of $E1$ PSF, and so on. However, sensitivity tests on these quantities, reported in the following subsections, indicate that this is not the case.

Since the sensitivity to other parameters of the simulations is rather weak (see below), we can make rather strong restrictions on values of the amplitude C. Comparisons presented in this subsection favor $C \simeq 0.5$–1.5×10^{-8} MeV^{-3} for all but Mo isotopes. Larger values of $C \simeq 2$–3.5×10^{-8} MeV^{-3} are then needed for Mo isotopes. This trend could indicate a dependence of the $M1$ low-ε_γ limit on quantities like deformation or mass number A. In reality, a possible dependence on the deformation seems not to be well pronounced as the two tested Mo isotopes require a similar value of C while having

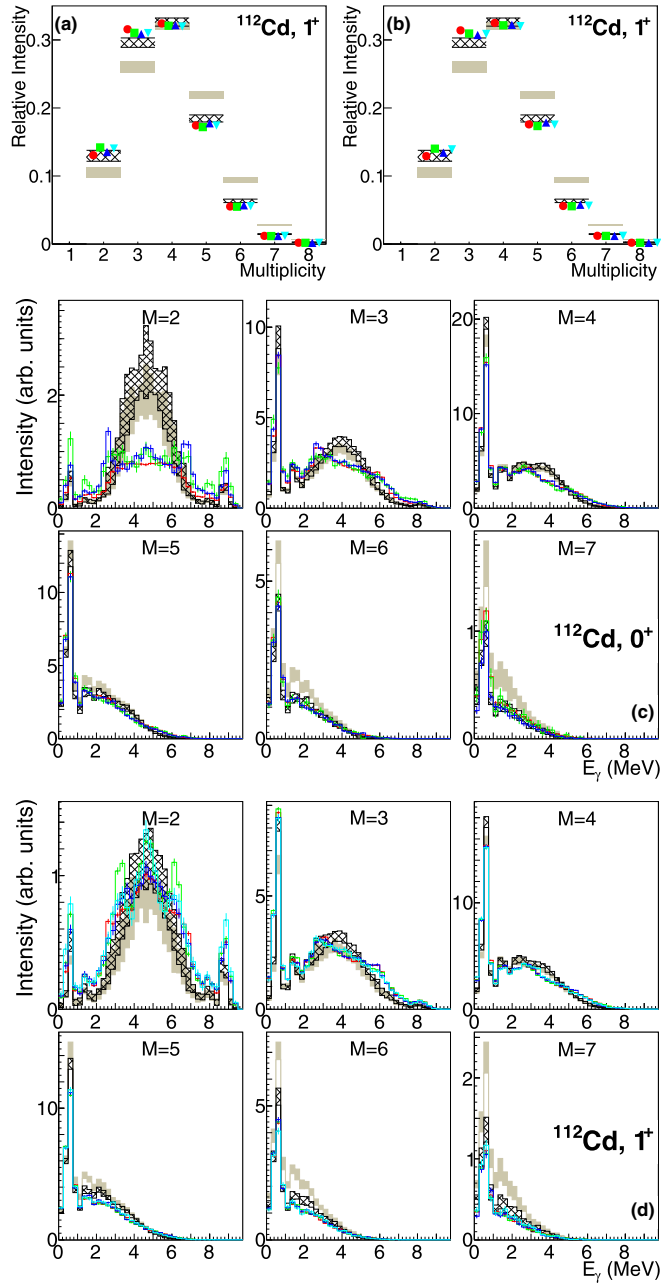

FIG. 5. The MD and MSC spectra from decay of 0^+ and 1^+ resonances in ^{112}Cd. The color symbols correspond to experimental data, the black hatched area and the gray band to predictions from simulations with $C = 1 \times 10^{-8}$ MeV^{-3} and $C = 3 \times 10^{-8}$ MeV^{-3}, respectively.

rather different predicted deformation parameters β_{20}, listed in Table I. In addition, the description of Cd data – with a deformation similar to that of ^{98}Mo – requires much lower C value, similar to well-deformed isotopes of Gd, Dy, and U. This deformation dependence will be further discussed in Sec. V.

We note that checks of consistency of various PSFs models with experimental MSC spectra in original works listed in Table I systematically indicated that a low-ε_γ PSF

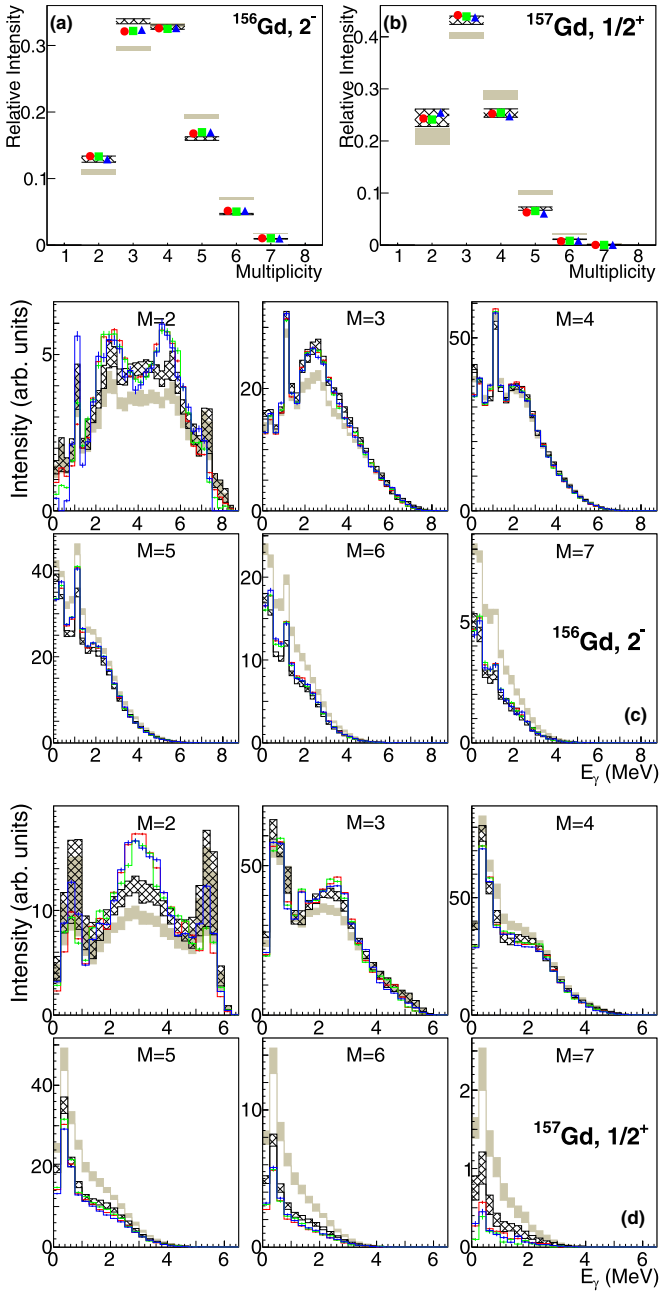

FIG. 6. The same as in Fig. 5 from decay of resonances in two Gd isotopes.

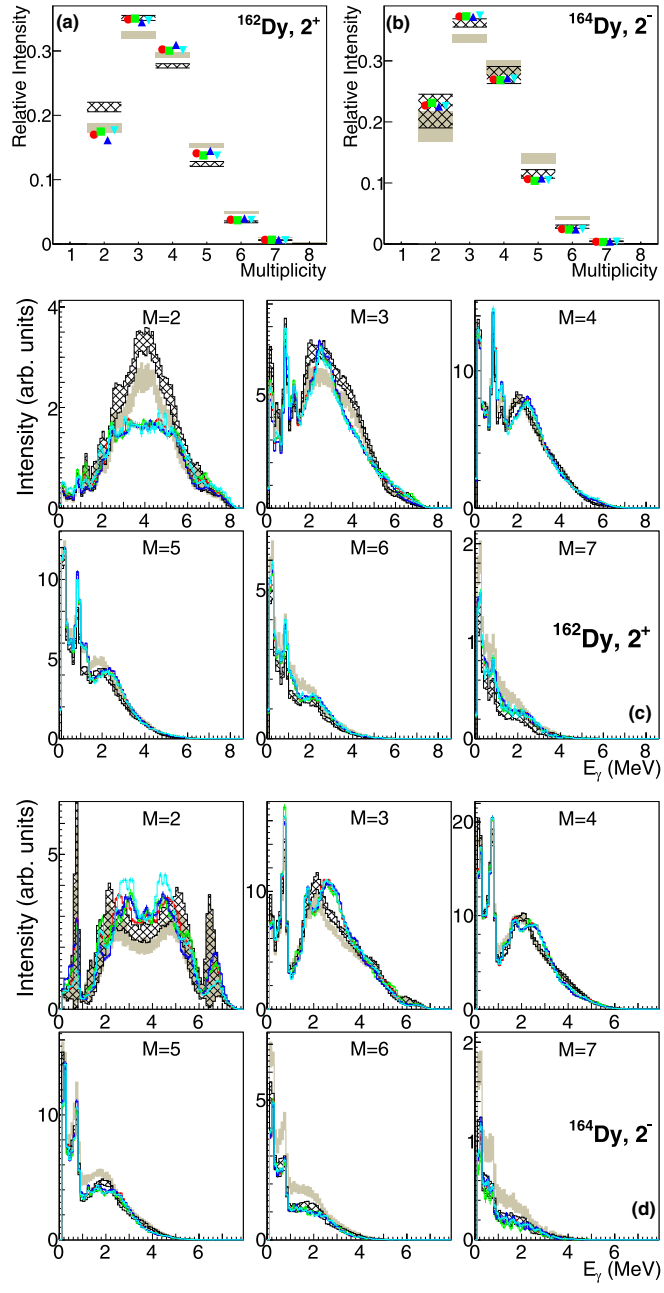

FIG. 7. The same as in Fig. 5 from decay of resonances in Dy isotopes.

enhancement cannot be significantly higher than that predicted by the GLO model [4,5], which gives a PSF of about 10^{-8} MeV^{-3} for $\varepsilon_\gamma = 0$ for decays of levels near S_n. This is fully consistent with the findings using the D1M + QRPA + 0lim model. Slightly higher low-ε_γ enhancement was probably allowed only in Mo isotopes, although it could hardly reach the zero-ε_γ limit of $\approx 3 \times 10^{-8}$ MeV^{-3} found in the present work. Higher allowed values of the zero-ε_γ limit in the present comparison of Mo isotopes can be associated with significantly different PSFs shapes compared to those tested in Refs. [44,45].

We have one additional comment to ^{96}Mo. The fluctuations in predicted MDs are significantly higher in the decay of negative than positive-parity resonances, see Fig. 2. These higher fluctuations are, at least partly, caused by fluctuations of a limited number of high-ε_γ $E1$ primary transitions to (positive-parity) levels at low excitation energy. Due to the high value of $E1$ PSF for $\varepsilon_\gamma \gtrsim 5$ MeV, these transitions are expected to play a significant role in the decay. In the decay of positive-parity resonances the absence of negative-parity levels below excitation energy of about 2 MeV leads to the elimination of fluctuations due to what would be high-ε_γ $E1$ transitions. Fluctuations in the experimental MDs from negative-parity

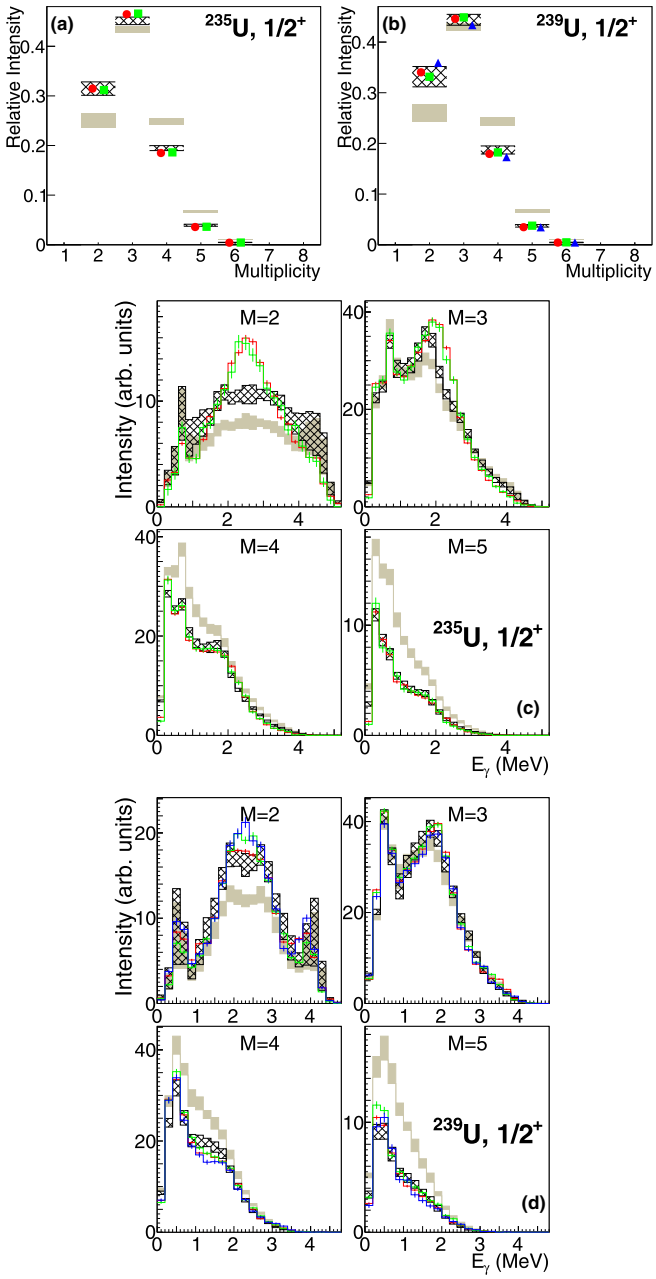

FIG. 8. The same as in Fig. 5 from decay of $1/2^+$ resonances in odd U isotopes.

^{96}Mo resonances are significantly smaller than in simulations. The similarity of experimental MD from different resonances is likely a consequence of the fact that the spin assignment is available only for a very restricted number of negative-parity resonances and the MD itself was used in the spin assignment [65]. The resonances showing some deviation from the average MD were kept with indefinite spin.

To conclude, although the agreement between experiment and predictions with the global D1M + QRPA + 0lim model is not always perfect, and, not surprisingly, better agreement can be reached with adjusted models or parameters – see original papers with an analysis of MSC spectra listed in Table I – these predictions are a significant improvement compared to other widely used PSFs models, see Sec. V.

B. Sensitivity to broadening width Γ_{M1}

The simulated spectra can be sensitive to different adopted values of the empirical broadening width Γ_{M1} applied to the D1M + QRPA predictions, especially if there is a pronounced resonance structure in the PSF at $\varepsilon_\gamma < S_n$. The most pronounced structure at these ε_γ is the so-called scissors mode in deformed nuclei, located at $\varepsilon_\gamma \approx 2$–3 MeV [10,66]. The mode strongly affects the predicted MSC spectra, see papers on deformed nuclei listed in Table I. A comparison between the D1M + QRPA model and NRF data indicated that the location of the mode is reasonably predicted [10]. A similar conclusion can be made also from MSC spectra, see Figs. 7 and 8 and Supplemental Material [59]. However, the broadening width was somewhat arbitrary adjusted to $\Gamma_{M1} = 0.5$ MeV in the model due to the lack of constraining experimental data.

To check the sensitivity of predictions to Γ_{M1} we simulated the MD and MSC spectra also with $\Gamma_{M1} = 2$ MeV. Predictions with these two Γ_{M1} values are compared in Figs. 9 and 10 for a few deformed Gd and U isotopes, respectively; more nuclei are compared in the Supplemental Material [59]. The MD spectra are not strongly affected by changes in Γ_{M1}. However, larger Γ_{M1} makes the predicted bumps at $\varepsilon_\gamma \approx 2$–3 MeV in the MSC spectra, especially for $M = 2$ and 3, too small. The effect is clearly seen especially in nuclei where the energy of the scissors mode is close to $S_n/2$.

We conclude that the $\Gamma_{M1} \approx 0.5$ MeV seems to be a reasonable choice, at least for deformed nuclei. For spherical and quasispherical nuclei the predicted MSC spectra are virtually insensitive to the adopted value of Γ_{M1}, see Supplemental Material [59]. In these nuclei the only relevant resonance structure in $M1$ is the spin-flip (SF) mode at energies 7–9– MeV and the influence of the Γ_{M1} on MSC spectra appears to be small for that high resonance energies.

C. Sensitivity to low-ε_γ limit of $E1$ PSF

A range of values of parameters f_0 and ε_0, describing the phenomenological low-ε_γ behavior of the $E1$ PSF, see Eq. (1), was proposed in Sec. II. All above-discussed simulations were performed with $f_0 = 1 \times 10^{-10}$ MeV^{-4} and $\varepsilon_0 = 3$ MeV that correspond to the lower low-ε_γ $E1$ PSF limit proposed in Ref. [11]. To check the influence of the $E1$ behavior on predictions, we also performed simulations with the upper low-ε_γ limit proposed in Ref. [11], $f_0 = 5 \times 10^{-10}$ MeV^{-4} and $\varepsilon_0 = 5$ MeV.

The upper $E1$ PSF limit is even for primary transitions smaller than (or at most comparable to) the required low-ε_γ $M1$ PSF limit given by the parameter C listed in Table I. In addition, as evident from Eq. (1) the $E1$ contribution further decreases for transitions de-exciting levels at lower excitation energies. It can thus be expected that the influence of different tested low-ε_γ $E1$ PSF limits is not significant. This expectation was confirmed for all surveyed nuclei, see examples shown in Fig. 11 and additional figures in the Supplemental Material [59].

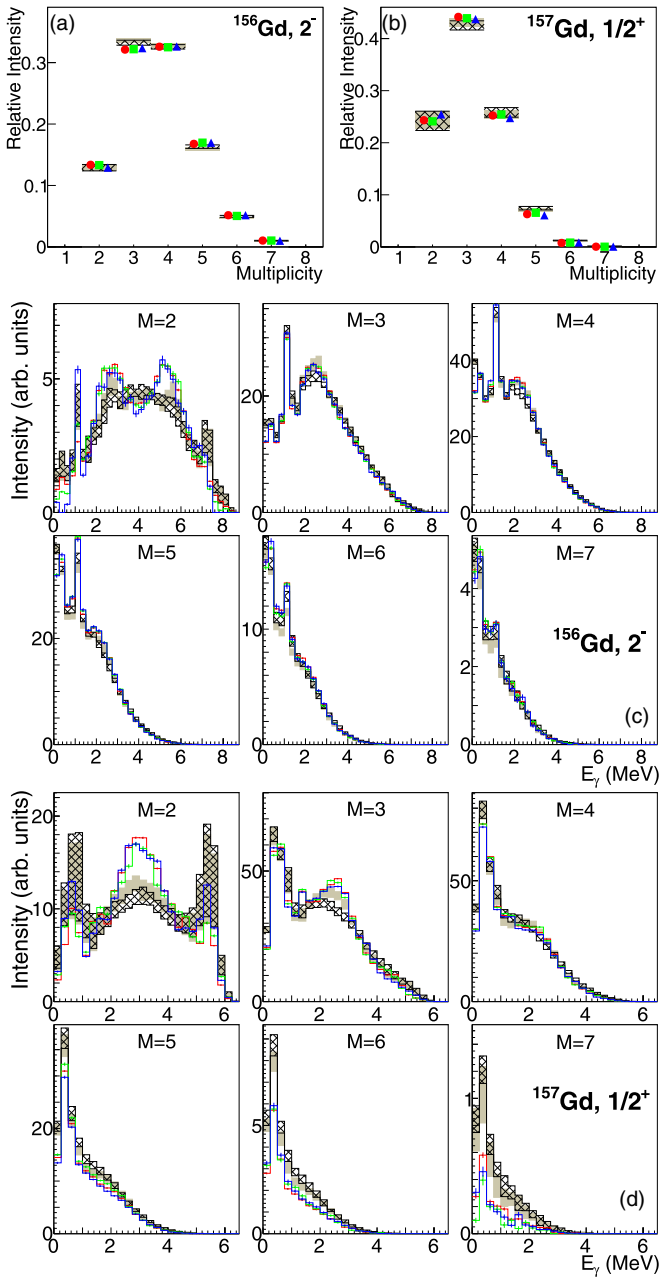

FIG. 9. The same as in Fig. 6 but for two different values of Γ_{M1}. The black hatched area corresponds to $\Gamma_{M1} = 2$ MeV and the gray band to $\Gamma_{M1} = 0.5$ MeV; $C = 1 \times 10^{-8}$ is adopted in both cases.

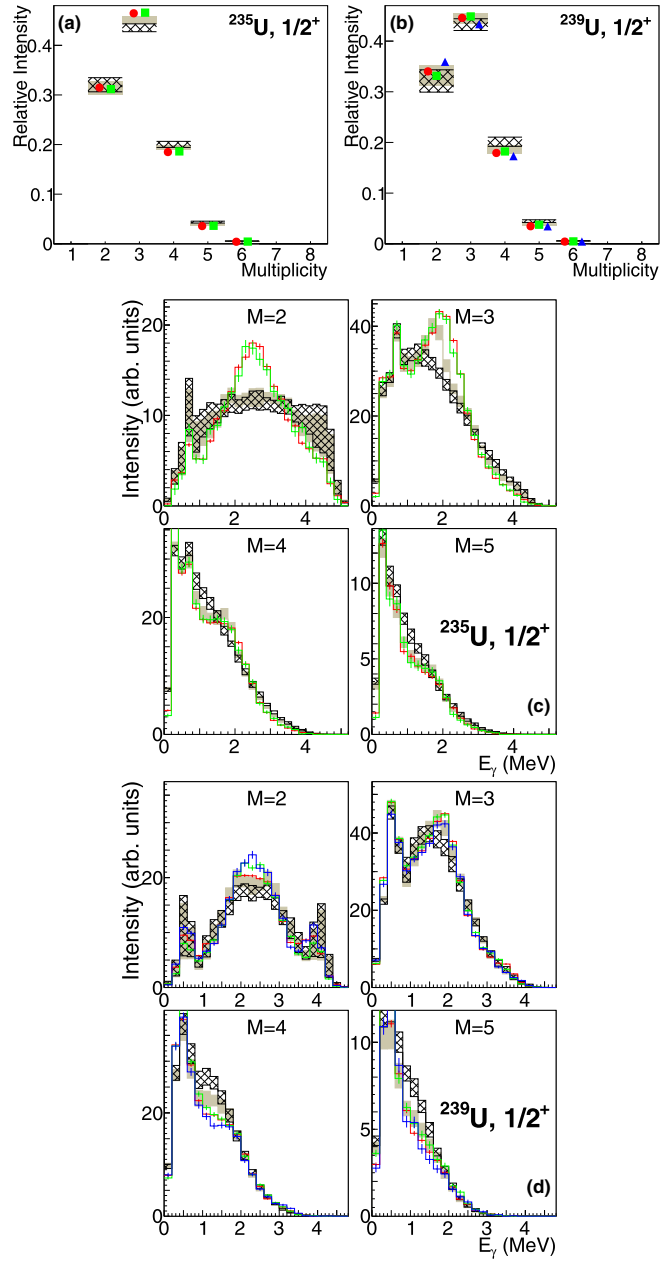

FIG. 10. The same as in Fig. 9 but for U isotopes.

The increase of the $E1$ limit leads to a small shift in the MD toward higher values. The value of C required to describe experimental data with the higher $E1$ PSF limit is thus slightly smaller, at maximum by $\simeq 3 \times 10^{-9}$ MeV^{-3} than that listed in Table I. Such a change corresponds to the difference in the zero-ε_γ limit for primary transitions.

D. Sensitivity to level density models

As mentioned above, the observables compared in this paper come from a complicated interplay between the PSFs and LD. Unfortunately, the actual LD is not well known. The sensitivity to different LD models thus needs to be analyzed. All simulations presented above were performed with the microscopically based HFB plus combinatorial approach to the LD [63]. To test the sensitivity to the adopted LD model, we also consider here the CT model [64] as recommended by RIPL-3. This model gives LDs similar to the CT model of Ref. [67].

The MD and MSC spectra with both tested LD models are compared in Figs. 12 to 14 for a sample of cases; more figures can be found in the Supplemental Material [59]. The CT model gives a smaller number of levels at all energies below S_n compared to the combinatorial one. The highest difference

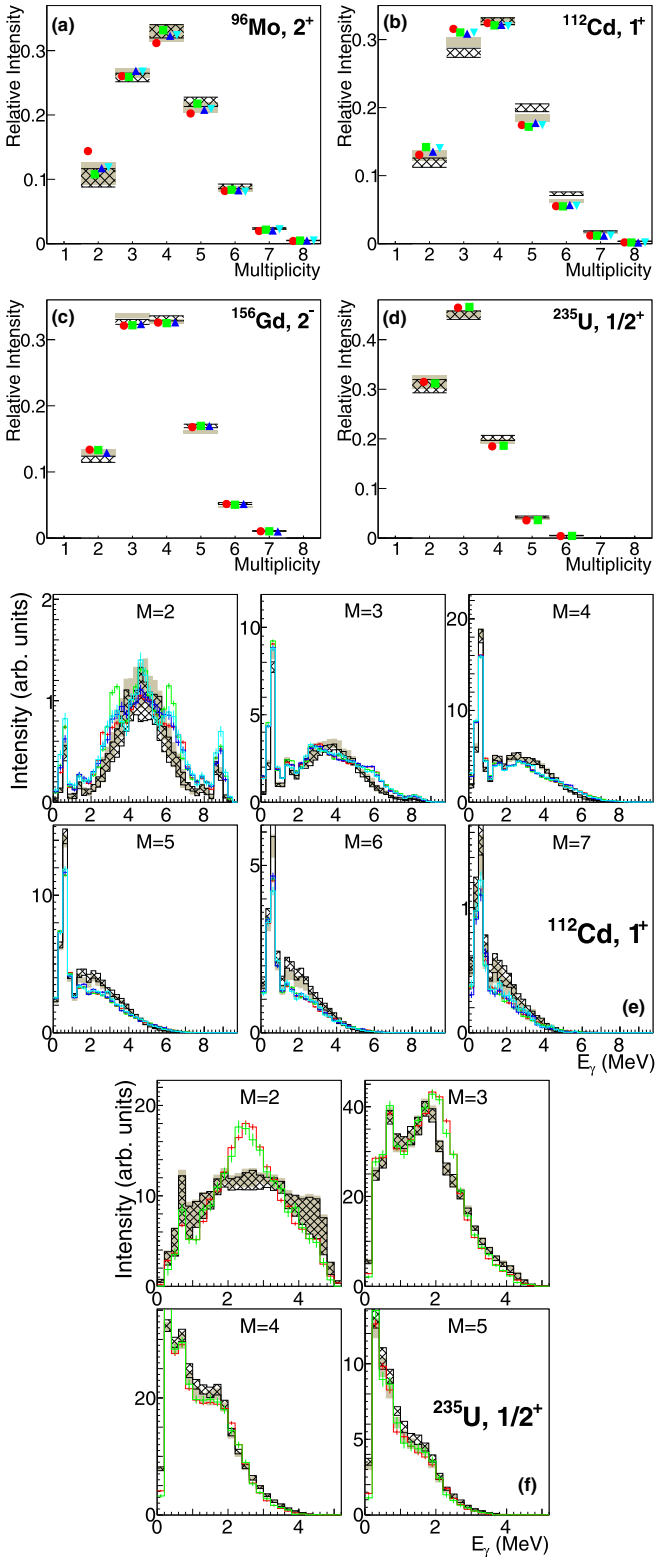

FIG. 11. Comparison between experimental and simulated MD and MSC spectra with different $E1$ low-ε_γ limits. Gray bands correspond to the lower $E1$ zero-ε_γ limit and the black hatched area to the upper $E1$ zero-ε_γ limit, see text; $C = 3 \times 10^{-8}$ MeV^{-3} is adopted for ^{96}Mo while $C = 1 \times 10^{-8}$ MeV^{-3} for all other isotopes.

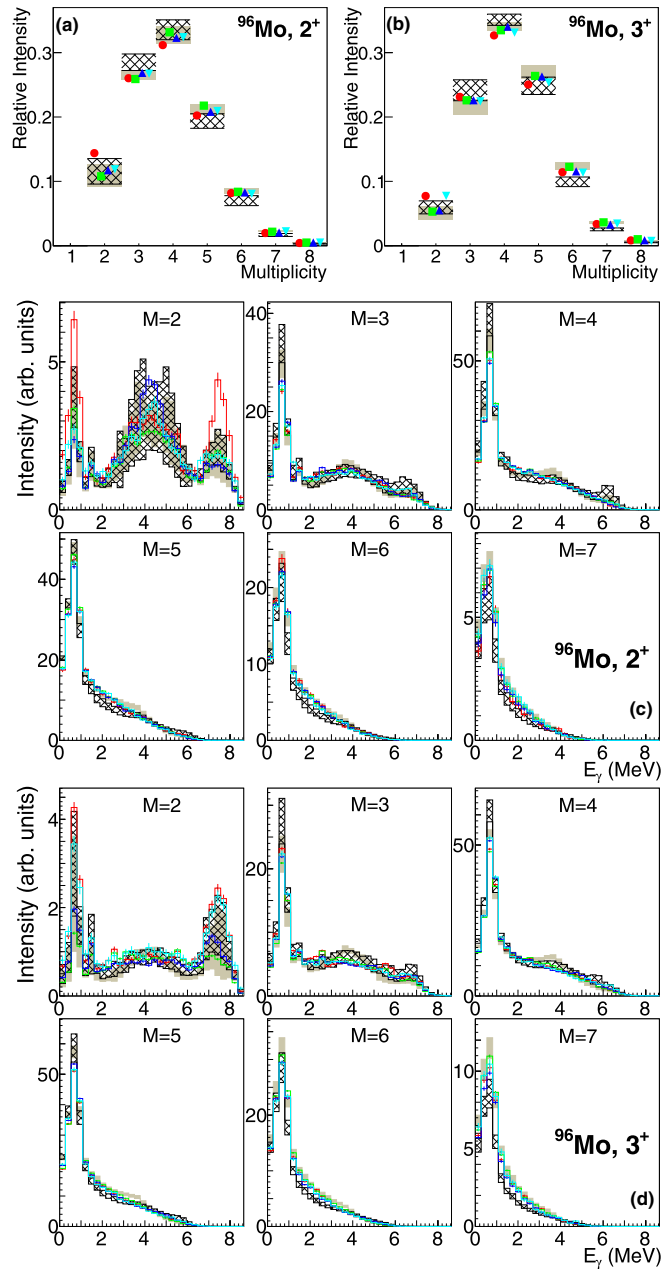

FIG. 12. Comparison between experimental and simulated MD and MSC spectra with different LD models in ^{96}Mo. The gray bands correspond to the combinatorial LD model while the black hatched area to the CT LD model; $C = 3 \times 10^{-8}$ MeV^{-3} was adopted.

occurs near $S_n/2$. This feature leads to a shift of the predicted MD to lower values when compared to combinatorial LD model for fixed PSFs. Such a shift is clear for all nuclei except ^{112}Cd, where the multiplicity for $M = 2$ does not exactly follow the trend. However, even in this nucleus the shift is visible for $M > 2$.

In general, predictions with different LD models may change also the shape of the MSC spectrum for a fixed

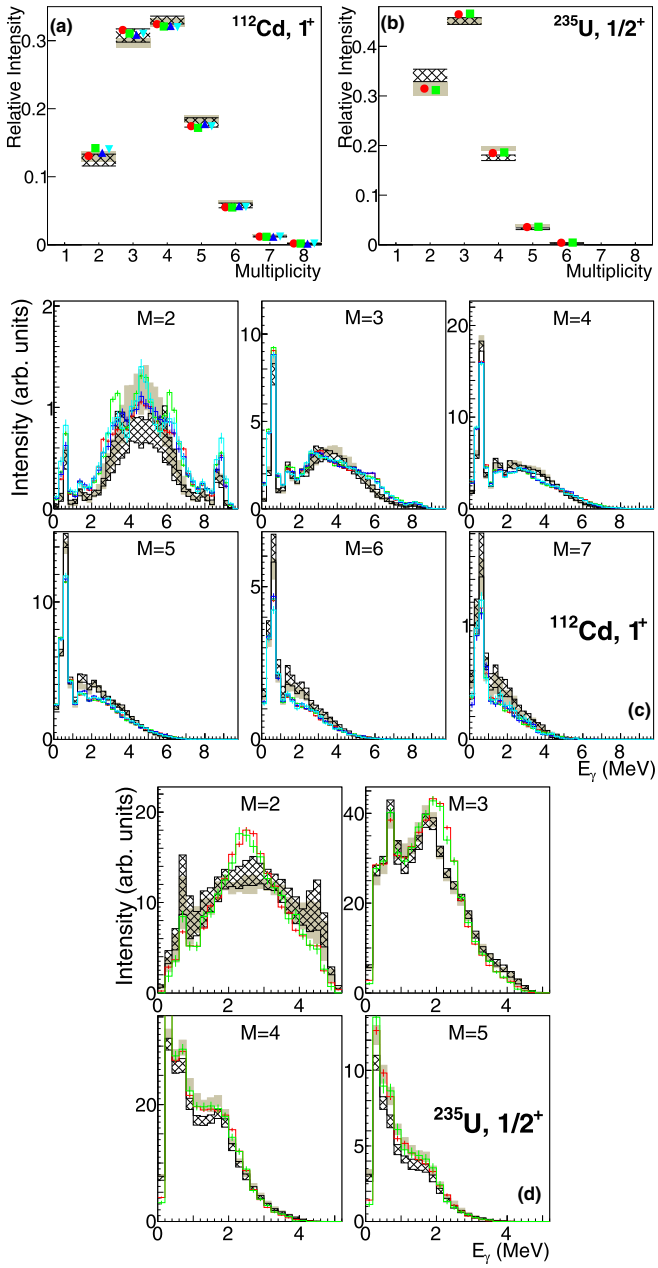

FIG. 13. The same as in Fig. 12 but for resonances in ^{112}Cd and ^{235}U isotopes; $C = 1 \times 10^{-8}$ MeV^{-3} was adopted.

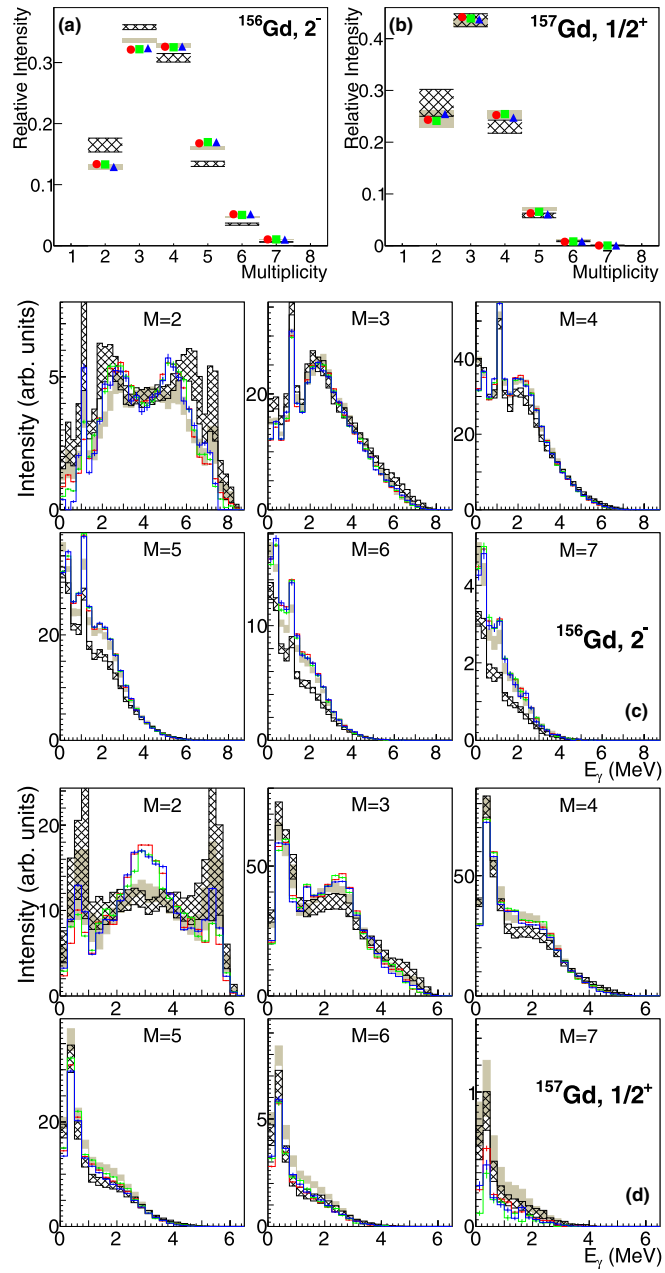

FIG. 14. The same as in Fig. 12 but for resonances in Gd isotopes; $C = 1 \times 10^{-8}$ MeV^{-3} was adopted.

multiplicity M. Such a change is evident especially for $M =$ 2–4 in rare-earth nuclei, see Fig. 14 for illustration for two Gd isotopes and the Supplemental Material [59] for other rare-earth nuclei. The most pronounced effect seems to be a suppression of the bump arising from the scissors mode. As a result, predictions with the CT model do not satisfactorily reproduce the MSC spectral shapes in well-deformed rare-earth nuclei. This observation is consistent with findings presented in original papers from analysis of the MSC spectra using the CT LD models with the parametrization from Refs. [67,68]. These findings strongly indicate that the CT model is not appropriate for the description of LD in well-deformed rare-earth nuclei.

In Mo, Cd, and U isotopes we usually cannot decide which of the tested LD models describes the experimental MSC spectral shape better. The reproduction of experiment is sometimes not perfect with any of the models. In general, to reproduce fairly experimental data in these elements using the CT LD model the value of the C parameter needs to be increased by a factor of about 1.5 with respect to the values obtained with the combinatorial LD model listed in Table I.

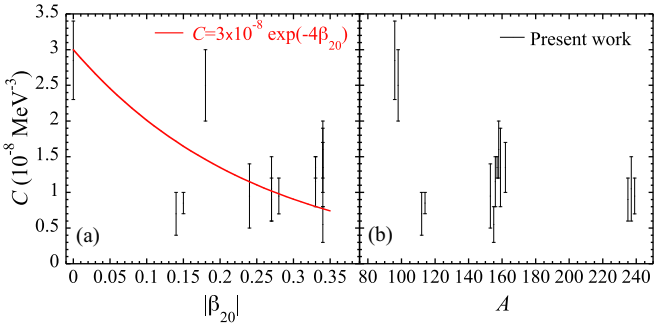

FIG. 15. Parameter C as extracted from the analysis of the MSC spectra and listed in Table I as a function of (a) the D1M quadrupole deformation parameter β_{20} and (b) the atomic mass A. Also shown is an exponential function $C = 3 \times 10^{-8} \exp(-4\beta_{20})$ MeV^{-3} in (a), see text for details. When different resonance spins with well-defined values of C are available, the interval compatible with all values is shown in the figure.

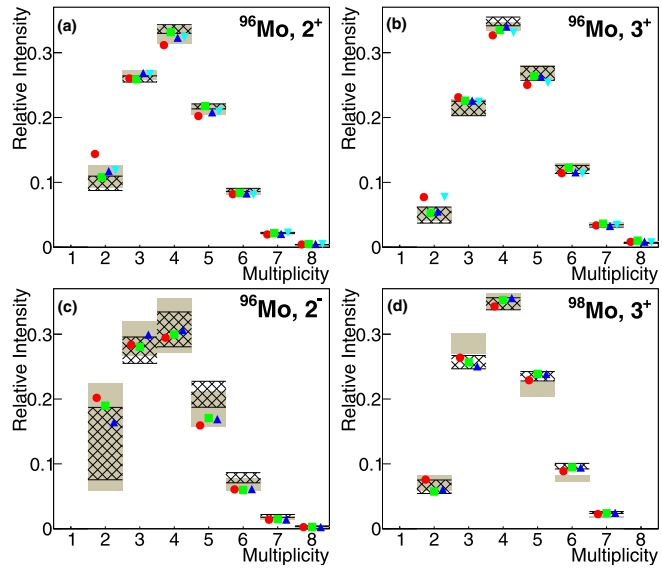

FIG. 16. A comparison of the experimental MD for Mo isotopes with predictions using the D1M + QRPA + 0lim model with the C value from the proposed global systematics, $C = 3 \times 10^{-8}$ MeV^{-3} for ^{96}Mo and $C = 1.5 \times 10^{-8}$ MeV^{-3} for ^{98}Mo (gray band), and using the GLO+SF model (black hatched area).

V. DISCUSSION

A. Constraints on low-ε_γ $M1$ limit

In the previous section we showed that the zero-ε_γ $M1$ PSF limit could be relatively well constrained from the analysis of the MD and MSC spectra. More precisely, the allowed value of C can be determined for individual nuclei with a relatively good accuracy of typically 1×10^{-8} MeV^{-3} if all other inputs (LD, low-ε_γ $E1$ PSF) are fixed, see Table I.

The SM calculations on light $A \lesssim 80$ nuclei [26–29] suggest that the amplitude of the zero-ε_γ $M1$ limit decreases with increasing nuclear deformation β_{20}, part of this strength being transferred to higher energies in the $\varepsilon_\gamma \simeq$ 2–3 MeV range where the scissors mode appears for deformed nuclei.

The deformation dependence of C from values listed in Table I, based on the combinatorial LD model, is shown in Fig. 15(a) together with a simple exponential trend. As discussed in Sec. IV D the CT LD model would require C values higher by ≈50%. Some outliers from a smooth dependence of C on deformation – ^{98}Mo with $\beta_{20} = 0.18$ and Cd isotopes with $\beta_{20} \simeq 0.15$ – are clearly observed in Fig. 15(a). However, it should be kept in mind that predicted deformations are open to theoretical uncertainties and that different interactions may predict rather different values. In particular, HFB calculations based on the D1S Gogny interaction predict a ground-state deformation of ^{98}Mo to be only $\beta_{20} \simeq 0.05$. Mass models based on various Skyrme interactions then predict deformations ranging between 0.17 and 0.25 for ^{98}Mo [53]. A similar discussion could be made for ^{96}Mo and Cd isotopes. All in all, on the one hand, no clear deformation dependence of the low-ε_γ $M1$ enhancement, as suggested by some SM calculations, can be deduced from the present analysis, but on the other hand, due to the uncertainties on the determination of the quadrupole deformation, such a dependence may well be present. To make more solid conclusion about such dependence, more experimental data, especially for spherical and quasi-spherical nuclei are needed.

In addition to the SM calculations, relevant experimental signatures of the low-ε_γ strength have been gathered through the so-called Oslo method [29,39]. Data processed by this method favor the presence of a strong low-ε_γ enhancement mainly for nuclei with $A \lesssim 105$, so that the extracted values of C in Table I might actually reflect rather a mass than deformation dependence of the C parameter. The mass dependence based on values of C in Table I is shown in Fig. 15(b). Additional MSC data for nuclei with mass below $A \approx 105$ would be needed to shed light on such a mass dependence. Unfortunately, the MSC data for nuclei with a relatively low LD, which includes almost all nuclei with $A \lesssim 90$, may not be very restrictive due to involved fluctuations and the limited number of resonances that can be measured with sufficient statistics.

To summarize, the presence of a nonnegligible $M1$ low-ε_γ strength is favored in all cases from analysis of MSC spectra, but it remains difficult to draw conclusions on its exact deformation or mass dependence. As proposed in Ref. [11], a lower value of $C = 1 \times 10^{-8}$ MeV^{-3} and upper value of $C = 3 \times 10^{-8}$ MeV^{-3} seems reasonable. For the time being we propose to consider in the D1M + QRPA + 0lim systematics, used together with the combinatorial LD model, the lower limit, $C = 1 \times 10^{-8}$ MeV^{-3}, for all nuclei with $A \gtrsim 105$. For lighter nuclei we propose a simple deformation dependence $C = 3 \times 10^{-8} \exp(-4\beta_{20})$ MeV^{-3}. Future theoretical and experimental work should help us in fine tuning of mass and/or deformation dependencies.

A comparison of D1M + QRPA + 0lim simulations for values of C from this systematics can be found in Figs. 2 to 8 with the exception of ^{98}Mo. The prediction for MD and MSC spectra with the recommended value of $C \simeq 1.5 \times 10^{-8}$ MeV^{-3} for ^{98}Mo are given in Figs. 16(d) and 18, respectively.

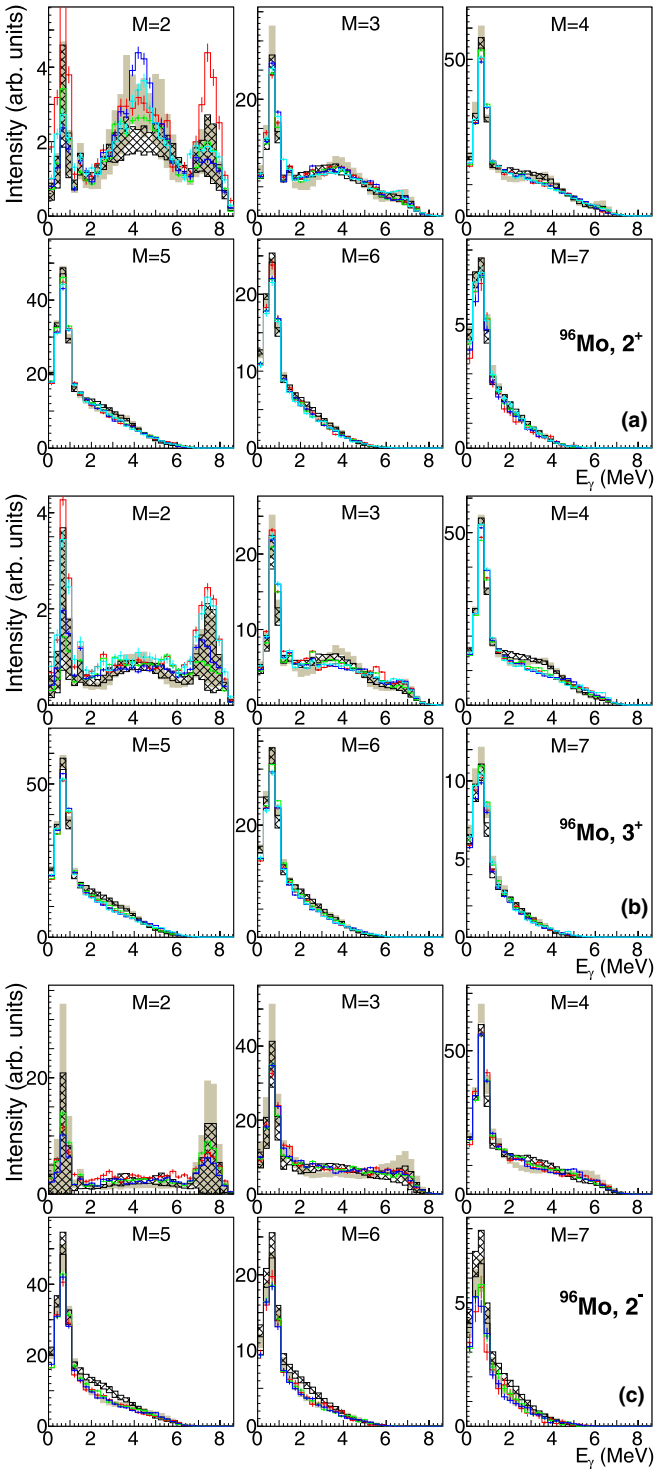

FIG. 17. Comparison of MSC predictions for ^{96}Mo with D1M + QRPA + 0lim model with C from proposed global systematics, $C = 3 \times 10^{-8}$ MeV^{-3} (gray band), and with the GLO + SF model (black hatched area).

B. Comparison to recommended PSF model

To emphasize the quality of the D1M + QRPA + 0lim model, we compare for a few isotopes in Figs. 16 to 21 experimental data with predictions from above-proposed

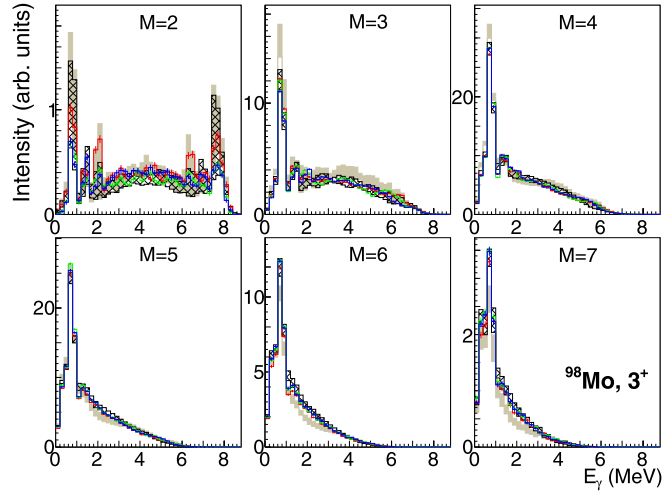

FIG. 18. Comparison of MSC predictions for 3$^+$ resonances in ^{98}Mo with D1M + QRPA + 0lim model with C from proposed global systematics, $C = 1.5 \times 10^{-8}$ MeV^{-3} (gray band), and GLO + SF model (black hatched area).

systematics and from probably the most widely used combination of the PSFs models to date – the GLO for $E1$ and the SF $M1$ of Refs. [4,5]. This combination is recommended by the RIPL-3 database [5], despite some known shortcomings in the description of γ-ray data below S_n such as the systematic underestimate of the average radiative widths [11]. All shown predictions with the GLO + SF PSFs in the paper were performed with the combinatorial LD model. Figures for all isotopes and resonance spins with this model combination can be found in the Supplemental Material [59] where we also show predictions of the GLO + SF PSFs combined with the CT LD model.

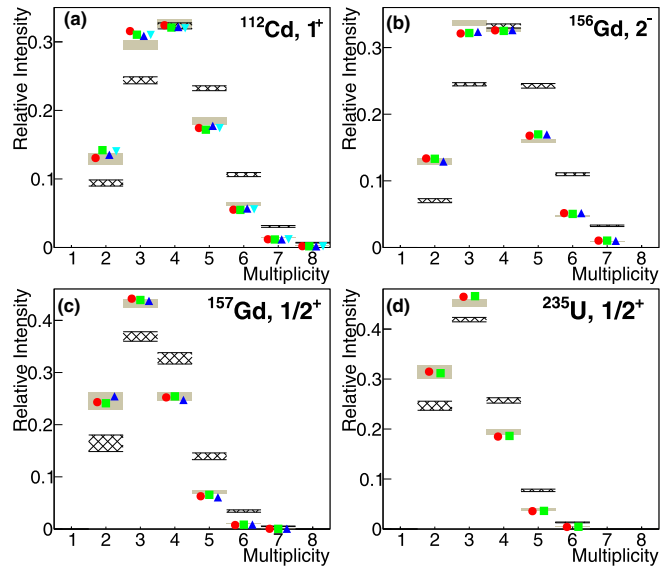

FIG. 19. The same as in Fig. 16 but for different isotopes. The proposed systematics of C gives $C = 1 \times 10^{-8}$ MeV^{-3} for all shown isotopes.

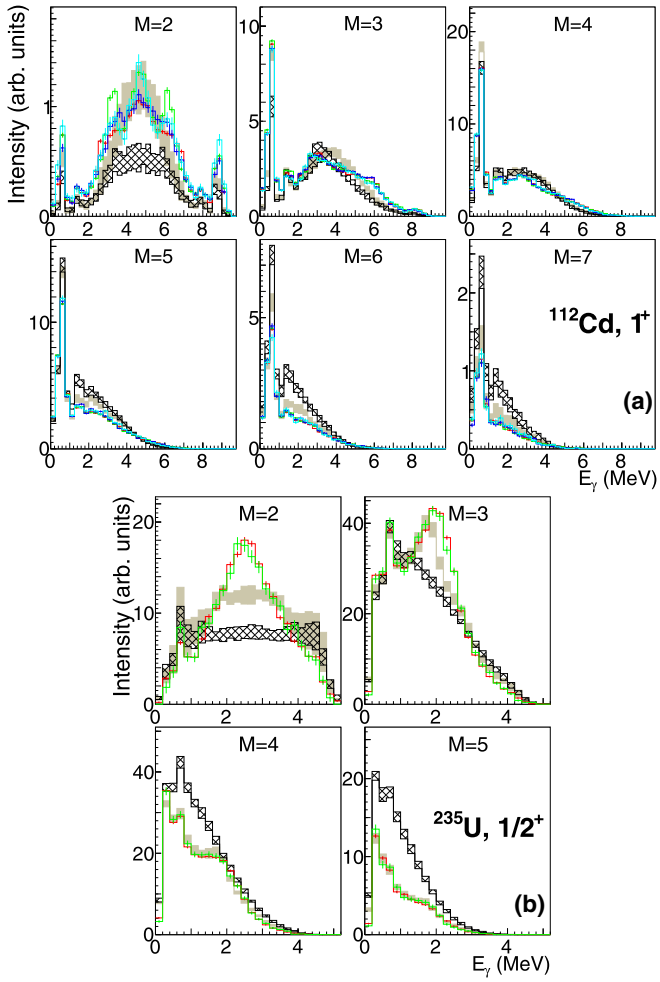

FIG. 20. The same as in Fig. 17 but for ^{112}Cd and ^{235}U. The proposed systematics of C gives $C = 1 \times 10^{-8}$ MeV^{-3} for both these isotopes.

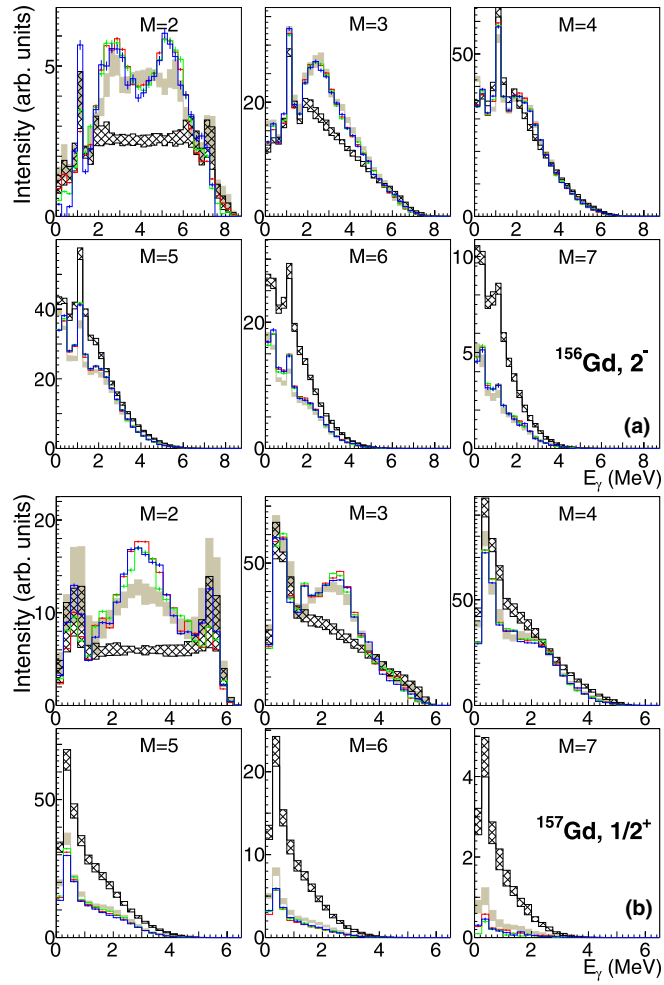

FIG. 21. The same as in Fig. 17 but for two Gd isotopes. The proposed systematics of C gives $C = 1 \times 10^{-8}$ MeV^{-3} for both these isotopes.

The GLO + SF PSFs combination can evidently give reasonable predictions of the MSC spectra in some cases, as illustrated for both Mo isotopes in Figs. 16 to 18. However, for all other tested nuclei the predictions do not describe experimental data satisfactorily, regardless of the LD model adopted. The main reason for the disagreement in well-deformed nuclei is the missing contribution from the $M1$ scissors mode at $\varepsilon_\gamma \approx 2$–3 MeV. In Cd nuclei the reason for the discrepancies is less clear. It might again come from the absence of the $M1$ strength at $\varepsilon_\gamma \ll S_n$. Nonetheless, this explanation might not be correct as in Mo isotopes the GLO + SF combination gives a reasonable description of the experiment.

Despite the absence of the significant $M1$ strength below S_n in the GLO + SF model, the predicted MD is similar to that from the D1M + QRPA + 0lim model with $C = 3 \times 10^{-8}$ MeV^{-3}. This is likely a consequence of the compensation of the low-ε_γ $M1$ contribution in the D1M + QRPA + olim model by the nonzero PSF limit for $\varepsilon_\gamma = 0$ included in the $E1$ GLO model.

VI. APPLICATION TO THE NEUTRON CAPTURE RATES OF ASTROPHYSICAL INTEREST

Radiative neutron capture cross sections play a fundamental role in most of the nucleosynthesis processes called for to explain the origin of the elements heavier than iron in the Universe [1,69]. Most of the nucleosynthesis calculations up to now were performed with neutron capture rates obtained with the phenomenological PSFs, such as the GLO + SF PSF models recommended by RIPL-3 [4,5].

Figure 22 illustrates in the (N, Z) plane the ratios of the Maxwellian-averaged cross sections (MACSs) at a temperature $T = 10^9$ K (typical of the r-process nucleosynthesis [1]) obtained with the D1M + QRPA + 0lim model with the C dependence proposed in Sec. V A to those obtained with the widely used GLO + SF model [4,5]. The calculations were performed with the TALYS reaction code [70] on the basis of the D1M masses [60] and HFB plus combinatorial LD model [63].

When approaching the neutron drip line, the MACS calculated with the D1M + QRPA + 0lim model is larger than the one obtained with the traditional GLO + SF PSF model

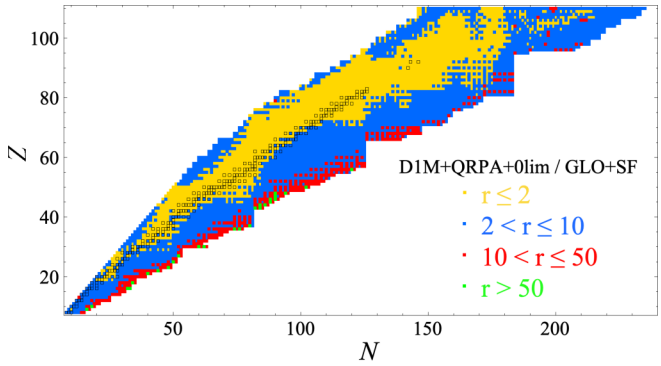

FIG. 22. Color-coded representation in the (N, Z) plane of the ratio of the (n, γ) Maxwellian-averaged cross sections at $T = 10^9$K obtained with the present recommended D1M + QRPA + 0lim to the one obtained with the GLO+SF PSF recommended in RIPL-3 [4,5]. Open black squares correspond to the stable nuclei and very long-lived actinides. All nuclei with $8 \leqslant Z \leqslant 110$ lying between the neutron and proton drip lines predicted by the D1M mass model are included.

by a factor up to about 50 (and even more for a few exotic neutron-rich nuclei). The most significant effects responsible for such an increase of the MACS are (i) the low-energy $E1$ strength predicted for neutron-rich nuclei by the D1M + QRPA approach (as discussed in Ref. [9]) and (ii) the low-energy $M1$ strength found in both the $\varepsilon_\gamma \to 0$ region and the scissors mode. Similar results with even larger increase of the rates were found in Ref. [11], where the D1M + QRPA + 0lim $M1$ PSF was used with larger values of the $M1$ zero-ε_γ limit, namely $C = 3 \times 10^{-8}$ MeV^{-3} for all nuclei. The newly constrained values of C, as proposed in Sec. V A tend to reduce the ratio with respect to the GLO + SF PSF model.

VII. CONCLUSION

Valuable theoretical predictions of nuclear dipole excitations in the whole chart are of great interest for different nuclear applications and especially nuclear astrophysics. In this paper we exploit a rich source of experimental data, namely multiplicity distributions and multistep γ cascade spectra resulting from the γ-decay of strong well-resolved resonances to learn about properties of the PSF at $\varepsilon_\gamma < S_n$. Specifically, we focus on testing and constraining the global PSFs model consisting of (i) the recent axially deformed HFB + QRPA calculations based on the D1M Gogny interaction and (ii) a phenomenological low-ε_γ contribution for the description of γ de-excitation process. Simulated MD and MSC spectra predicted by this model are compared with experimental counterparts from the DANCE detector, which are now available for 15 different isotopes ranging from Mo to U, in some cases for different initial resonance spins.

The PSF at $\varepsilon_\gamma \lesssim 5$ MeV in the D1M + QRPA + 0lim PSF model is dominated by (i) the low-ε_γ phenomenological $M1$ strength, taken as a simple exponentially decreasing function of the ε_γ as suggested by the SM calculations, and (ii) for well-deformed nuclei by the $M1$ scissors mode, which is consistently predicted by the D1M + QRPA calculations. For spherical nuclei, no scissors mode exists and the low-energy $E1$ limit may dominate in the $\varepsilon_\gamma \approx 2$–5 MeV range.

Experimental MD and MSC spectra are clearly sensitive to the low-ε_γ dipole PSF and can be used to test or further constrain existing global models such as the D1M + QRPA + 0lim one. We can conclude that the scissors mode location and strength is properly described by this model. We also test the broadening width Γ_{M1}, that describes the damping of collective motions including particularly the scissors mode. The MSC spectra are inconsistent with $\Gamma_{M1} \gtrsim 1$ MeV and well consistent with the adopted value of $\Gamma_{M1} = 0.5$ MeV.

The sensitivity to the $M1$ behavior at $\varepsilon_\gamma \lesssim 3$ MeV enables us to provide estimates of the parameter C, which describes the phenomenological zero-ε_γ $M1$ PSF limit, at least if all other PSFs and LD inputs are fixed. Tests are performed to study the impact of other PSFs and LD parameters. They reveal that uncertainties in the LD can lead to changes in the required C values which are estimated to be up to about 50%. However, some LD models seem to be inappropriate for certain mass regions. More specifically, as already mentioned in previous studies of MSC spectra, the CT model is found to be unable to reproduce spectral shapes of MSC data in well-deformed rare-earth nuclei.

The influence of other PSFs parameters to allowed value of C is found to be small. This is especially the case of the low-ε_γ $E1$ limit. Its small influence arises from the fact that the maximum tested $E1$ low-ε_γ limit is smaller than the required $M1$ PSF limit. Further, as majority of tested nuclei are well-deformed we cannot say much about correctness of the $E1$ predictions at $\varepsilon_\gamma \approx 2$–5 MeV due to the presence of the scissors mode. More data on spherical or quasispherical nuclei may shed light on the correctness of the $E1$ PSF in this ε_γ region.

The presence of a low-ε_γ $M1$ de-excitation strength, not included in the D1M + QRPA calculation of the PSF, is clearly favored in all nuclei, but it remains difficult to draw definite conclusions on its exact deformation or mass dependence. Future theoretical and experimental work should help in understanding these dependencies. In the meantime, a simple systematics is proposed for the $M1$ low-ε_γ PSF. Namely, we propose a constant value of $C = 1 \times 10^{-8}$ MeV^{-3} for all nuclei with $A \gtrsim 105$ and a simple deformation dependence $C = 3 \times 10^{-8} \exp(-4\beta_{20})$ MeV^{-3} for lighter nuclei. This systematics applied to the global D1M + QRPA + 0lim model in combination with the combinatorial LD model has been shown to give rather reasonable description of the MD and MSC spectra, though there is still room for improvement.

The D1M + QRPA + 0lim PSF may affect significantly the radiative neutron capture rates of astrophysical interest, in particular, for neutron-rich nuclei. The low-ε_γ contribution may increase the rates by a factor up to 50 for the most exotic nuclei close to the neutron drip line with respect to the rates obtained with the widely used GLO + SF PSF.

ACKNOWLEDGMENTS

This work was performed within the IAEA CRP F41032 on "Updating the Photonuclear data Library and generating a Reference Database for Photon Strength Functions."

S.G. acknowledges the support of the FRS-FNRS, S.V. the support of the Charles University via the UNCE/SCI/013 project. The project was also supported by the Czech Science Foundation under Grant No. 19-14048S.

[1] M. Arnould, S. Goriely, and K. Takahashi, Phys. Rep. **450**, 97 (2007).
[2] Y. Xu, S. Goriely, A. J. Koning, and S. Hilaire, Phys. Rev. C **90**, 024604 (2014).
[3] S. G. Kadmenskii, V. P. Markushev, and V. I. Furman, Sov. J. Nucl. Phys. **37**, 165 (1983).
[4] J. Kopecky and M. Uhl, Phys. Rev. C **41**, 1941 (1990).
[5] R. Capote *et al.*, Nucl. Data Sheets **110**, 3107 (2009).
[6] S. Goriely and E. Khan, Nucl. Phys. A **706**, 217 (2002).
[7] S. Goriely, E. Khan, and M. Samyn, Nucl. Phys. A **739**, 331 (2004).
[8] I. Daoutidis and S. Goriely, Phys. Rev. C **86**, 034328 (2012).
[9] M. Martini, S. Péru, S. Hilaire, S. Goriely, and F. Lechaftois, Phys. Rev. C **94**, 014304 (2016).
[10] S. Goriely, S. Hilaire, S. Péru, M. Martini, I. Deloncle, and F. Lechaftois, Phys. Rev. C **94**, 044306 (2016).
[11] S. Goriely, S. Hilaire, S. Péru, and K. Sieja, Phys. Rev. C **98**, 014327 (2018).
[12] G. Colò and P. Bortignon, Nucl. Phys. A **696**, 427 (2001).
[13] D. Sarchi, P. Bortignon, and G. Colò, Phys. Lett. B **601**, 27 (2004).
[14] N. Tsoneva and H. Lenske, Phys. Rev. C **77**, 024321 (2008).
[15] P. Papakonstantinou and R. Roth, Phys. Lett. B **671**, 356 (2009).
[16] O. Achakovskiy, A. Avdeenkov, S. Goriely, S. Kamerdzhiev, and S. Krewald, Phys. Rev. C **91**, 034620 (2015).
[17] D. Gambacurta, M. Grasso, and O. Vasseur, Phys. Lett. B **777**, 163 (2018).
[18] E. Litvinova, P. Ring, and V. Tselyaev, Phys. Rev. C **88**, 044320 (2013).
[19] I. A. Egorova and E. Litvinova, Phys. Rev. C **94**, 034322 (2016).
[20] D. Brink, Ph.D. thesis, University of Oxford, 1955.
[21] A. Voinov, E. Algin, U. Agvaanluvsan, T. Belgya, R. Chankova, M. Guttormsen, G. E. Mitchell, J. Rekstad, A. Schiller, and S. Siem, Phys. Rev. Lett. **93**, 142504 (2004).
[22] W. Furman, K. Niedzwiediuk, Y. Popov, R. Rumi, V. Salatsky, V. Tishin, and P. Winiwarter, Phys. Lett. B **B 44**, 465 (1973).
[23] R. Schwengner, S. Frauendorf, and A. C. Larsen, Phys. Rev. Lett. **111**, 232504 (2013).
[24] B. A. Brown and A. C. Larsen, Phys. Rev. Lett. **113**, 252502 (2014).
[25] K. Sieja, Phys. Rev. Lett. **119**, 052502 (2017).
[26] K. Sieja, EPJ Web of Conferences **146**, 05004 (2017).
[27] S. Karampagia, B. A. Brown, and V. Zelevinsky, Phys. Rev. C **95**, 024322 (2017).
[28] R. Schwengner, S. Frauendorf, and B. A. Brown, Phys. Rev. Lett. **118**, 092502 (2017).
[29] J. E. Midtbø, A. C. Larsen, T. Renstrøm, F. L. Bello Garrote, and E. Lima, Phys. Rev. C **98**, 064321 (2018).
[30] M. D. Jones *et al.*, Phys. Rev. C **97**, 024327 (2018).
[31] B. L.Berman, At. Data Nucl. Data Tables **15**, 319 (1975).
[32] IAEA, TECDOC-1178 (2000).
[33] H. Utsunomiya *et al.*, Phys. Rev. C **88**, 015805 (2013).
[34] V. Plujko, O. Gorbachenko, R.Capote, and P. Dimitriou, At. Data Nucl. Data Tables **123**, 1 (2018).
[35] R. Massarczyk, G. Rusev, R. Schwengner, F. Dönau, C. Bhatia, M. E. Gooden, J. H. Kelley, A. P. Tonchev, and W. Tornow, Phys. Rev. C **90**, 054310 (2014).
[36] N. Pietralla, P. von Brentano, R.-D. Herzberg, U. Kneissl, N. LoIudice, H. Maser, H. H. Pitz, and A. Zilges, Phys. Rev. C **58**, 184 (1998).
[37] M. Guttormsen *et al.*, Phys. Rev. C **71**, 044307 (2005).
[38] M. Guttormsen *et al.*, Phys. Rev. C **89**, 014302 (2014).
[39] Oslo database, Level densities and gamma-ray strength functions (2017), http://www.mn.uio.no/fysikk/english/research/about/infrastructure/OCL/nuclear-physics-research/compilation/.
[40] J. Kopecky, S. Goriely, S. Péru, S. Hilaire, and M. Martini, Phys. Rev. C **95**, 054317 (2017).
[41] S. Valenta, F. Becvar, J. Kroll, M. Krticka, and I. Tomandl, Phys. Rev. C **92**, 064321 (2015).
[42] M. Krtička, F. Bečvář, J. Honzátko, I. Tomandl, M. Heil, F. Käppeler, R. Reifarth, F. Voss, and K. Wisshak, Phys. Rev. Lett. **92**, 172501 (2004).
[43] M. Krtička, F. Bečvář, I. Tomandl, G. Rusev, U. Agvaanluvsan, and G. E. Mitchell, Phys. Rev. C **77**, 054319 (2008).
[44] S. A. Sheets *et al.*, Phys. Rev. C **79**, 024301 (2009).
[45] C. L. Walker *et al.*, Phys. Rev. C **92**, 014324 (2015).
[46] G. Rusev, M. Jandel, M. Krticka, T. A. Bredeweg, A. Couture, T. N. Taddeucci, and J. L. Ullmann, Phys. Rev. C **87**, 054603 (2013).
[47] J. Kroll *et al.*, Phys. Rev. C **88**, 034317 (2013).
[48] B. Baramsai *et al.*, Phys. Rev. C **87**, 044609 (2013).
[49] A. Chyzh *et al.*, Phys. Rev. C **84**, 014306 (2011).
[50] S. Valenta *et al.*, Phys. Rev. C **96**, 054315 (2017).
[51] J. L. Ullmann *et al.*, Phys. Rev. C **96**, 024627 (2017).
[52] S. Péru and H. Goutte, Phys. Rev. C **77**, 044313 (2008).
[53] S. Goriely, N. Chamel, and J. M. Pearson, Phys. Rev. C **93**, 034337 (2016).
[54] E. Algin, U. Agvaanluvsan, M. Guttormsen, A. C. Larsen, G. E. Mitchell, J. Rekstad, A. Schiller, S. Siem, and A. Voinov, Phys. Rev. C **78**, 054321 (2008).
[55] M. Heil, R. Reifarth, M. Fowler, R. Haight, F. Kappeler, R. Rundberg, E. Seabury, J. Ullmann, J. Wilhelmy, and K. Wisshak, Nucl. Instrum. Methods Phys. Res. A **459**, 229 (2001).
[56] R. Reifarth *et al.*, Nucl. Instrum. Methods Phys. Res. A **531**, 530 (2004).
[57] P. Losowski, C. Bowman, G. Russell, and S. Wender, Nucl. Sci. Eng. **106**, 208 (1990).
[58] M. Jandel *et al.*, Nucl. Instrum. Methods Phys. Res. B **261**, 1117 (2007), 19th International Conference on Application of Accelerators in Research and Industry, Ft Worth, TX, AUG 20–25, 2006.
[59] See Supplemental Material at http://link.aps.org/supplemental/10.1103/PhysRevC.99.044308 for details.
[60] S. Goriely, S. Hilaire, M. Girod, and S. Péru, Phys. Rev. Lett. **102**, 242501 (2009).
[61] C. Porter and R. Thomas, Phys. Rev. **104**, 483 (1956).
[62] F. Becvar, Nucl. Instrum. Methods Phys. Res. A **417**, 434 (1998).

[63] S. Goriely, S. Hilaire, and A. J. Koning, Phys. Rev. C **78**, 064307 (2008).
[64] A. Koning, S. Hilaire, and S. Goriely, Nucl. Phys. A **810**, 13 (2008).
[65] S. A. Sheets *et al.*, Phys. Rev. C **76**, 064317 (2007).
[66] K. Heyde, P. von Neumann-Cosel, and A. Richter, Rev. Mod. Phys. **82**, 2365 (2010).
[67] T. von Egidy and D. Bucurescu, Phys. Rev. C **80**, 054310 (2009).
[68] D. Bucurescu and T. von Egidy, Phys. Rev. C **72**, 067304 (2005).
[69] M. Arnould and K. Takahashi, Rep. Prog. Phys. **62**, 395 (1999).
[70] A. Koning and D. Rochman, Nucl. Data Sheets **113**, 2841 (2012).